

Performance Evaluation of LoRa for IoT Applications in Non-Terrestrial Networks via ns-3

Alessandro Traspadini, Michele Zorzi, Marco Giordani

Department of Information Engineering, University of Padova, Italy

Email: {traspadini, zorzi, giordani}@dei.unipd.it

Abstract—The integration of Internet of Things (IoT) and Non-Terrestrial Networks (NTNs) has emerged as a key paradigm to provide connectivity for sensors and actuators via satellite gateways in remote areas where terrestrial infrastructure is limited or unavailable. Among other Low-Power Wide-Area Network (LPWAN) technologies for IoT, Long Range (LoRa) holds great potential given its long range, energy efficiency, and flexibility. In this paper, we explore the feasibility and performance of LoRa to support large-scale IoT connectivity through Low Earth Orbit (LEO) satellite gateways. To do so, we developed a new ns3-LoRa-NTN simulation module, which integrates and extends the ns3-LoRa and ns3-NTN modules, to enable full-stack end-to-end simulation of satellite communication in LoRa networks. Our results, given in terms of average data rate and Packet Reception Ratio (PRR), confirm that LoRa can effectively support direct communication from the ground to LEO satellites, but network optimization is required to mitigate collision probability when end nodes use the same Spreading Factors (SFs) over long distances.

Index Terms—Non-Terrestrial Network (NTN); Long Range (LoRa); Internet of Things (IoT); ns-3.

I. INTRODUCTION

The global market for the Internet of Things (IoT) is expected to reach a value of around USD 11.1 trillion [1] in 2025, with approximately 75 billion connected units. To support this growth, current IoT connectivity solutions primarily rely on Low-Power Wide-Area Network (LPWAN) technologies such as Long Range (LoRa) [2], Narrowband-IoT (NB-IoT) [3], and SigFox [4], which offer a good compromise between coverage, power consumption, and throughput. However, as IoT deployments expand into rural regions, LPWANs face several limitations. First, LPWANs rely on existing cellular or dedicated network gateways, which are often unavailable or entirely absent in these regions. Moreover, while LPWANs scale well in dense urban deployments, extending coverage in vast and isolated rural areas is often impractical from both a technical and economic point of view. Additionally, remote areas may not have access to power/energy sources, which further complicates network deployment [5].

To address these limitations, recent studies have started to explore the integration of LPWANs with Non-Terrestrial Networks (NTNs) to support IoT applications [6]. In this solution, generally referred to as NTN-IoT [7], the IoT gateway is hosted onboard aerial/space nodes operating from the sky, especially Low Earth Orbit (LEO) satellites, to provide very large continuous and autonomous geographical coverage, even

in the absence of pre-existing terrestrial infrastructures. However, the existing literature primarily concentrates on urban areas and smart city use cases (e.g., [8]), with limited focus on rural or remote areas, which would benefit the most from this paradigm. For example, NTN-IoT can facilitate smart agriculture, e.g., precision farming via real-time monitoring of soil conditions, even in areas without cellular coverage. At sea, NTN-IoT allows maritime surveillance and monitoring, e.g., vessel tracking, weather alerts, and monitoring of fishing activities, when terrestrial signals are unavailable. Furthermore, NTN-IoT ensures resilient, always-on communication during or after disasters, when ground infrastructure may be damaged or inaccessible, to provide coordination of rescue teams, especially in remote or hard-to-reach areas.

The feasibility of direct satellite access from IoT devices has been explored in [9] and [10] using NB-IoT and LoRa, respectively. Additionally, Long Range–Frequency Hopping Spread Spectrum (LR-FHSS), a physical-layer enhancement of LoRa, has been proposed in [11] to improve the uplink performance in NTN scenarios. The 3rd Generation Partnership Project (3GPP) is also supporting this framework, and NB-IoT has been considered the leading candidate for NTN-IoT deployments, as explored in [12]. However, preliminary performance evaluations suggested that NB-IoT may not be optimal, especially in terms of link budget and delay [13]. Rather, the flexibility of LoRa permits to increase the communication range beyond the limits of NB-IoT, and turns out to be the best approach for LEO satellites. However, most of these studies focus primarily on the link layer, and introduce many assumptions and simplifications across the network stack.

In this work, we investigate the feasibility and end-to-end performance of NTN-IoT based on LoRa. Specifically, we analyze the data rate and Packet Reception Ratio (PRR) of the access link between IoT end nodes and a LEO satellite gateway, as a function of the altitude of the satellite, the antenna configuration, and the amount of traffic at the application. To do so, we use ns-3, one of the most accurate tools for network simulations. Although ns-3 includes the ns3-LoRa and ns3-NTN modules to simulate standalone LoRa and NTN scenarios, respectively, it does not natively integrate the two. To bridge this gap, we developed a new simulation module, called ns3-LoRa-NTN, that integrates the 3GPP NTN channel model into the LoRaWAN protocol stack. Our results show that, despite the more severe propagation environment in satellite networks, the flexibility of LoRa allows ground users to adjust the Spreading Factor (SF), and to communicate with

LEO gateways over long distances.

The remainder of the paper is organized as follows. In Sec. II we introduce our system model and the LoRa specifications. In Sec. III we present our ns-3 simulation framework. In Sec. IV we discuss the simulation results. Finally, conclusions are drawn in Sec. V.

II. SYSTEM MODEL

In this section we describe our scenario (Sec. II-A), review the main features of LoRa for IoT (Sec. II-B), and present our channel model (Sec. II-C).

A. Scenario

In this work, we consider a network with N LoRa End Devices (EDs), uniformly distributed across a circular area of size A_c . A single LEO satellite, acting as a LoRa gateway, is deployed at an altitude h , and communicates directly with the EDs through a directional antenna with a beamwidth θ . The antenna footprint on the ground forms a circular area of radius R_c given by

$$R_c = \tan(\theta/2) \cdot h. \quad (1)$$

The resulting service area is

$$A_c = R_c^2 \pi. \quad (2)$$

For a given ED spatial density ρ_d , the total number of EDs in the service area is computed as

$$N = \rho_d A_c. \quad (3)$$

The communication distance between an ED and the LEO satellite is determined by the slant range d , which depends on the ED position within the service area. As described in [14], this distance can be derived as

$$d = \sqrt{R_E^2 \sin^2(\alpha) + h^2 + 2hR_E - R_E \sin(\alpha)}, \quad (4)$$

where $R_E = 6371$ km is the Earth's radius, and α is the elevation angle between the ED and the satellite.

B. LoRa

In this study, we consider the case in which EDs communicate with the LEO satellite gateway using the LoRa technology. Specifically, LoRa is a proprietary physical layer modulation technique based on Chirp Spread Spectrum (CSS), which offers long-range, low-power connectivity, making it suitable for massive IoT deployments.

In CSS, data packets are modulated using a chirp signal/waveform whose frequency increases (up-chirp) or decreases (down-chirp) linearly over a fixed bandwidth B . The rate at which the frequency of the signal changes during the symbol duration, i.e., the chirp rate k , is given by

$$k = B/2^{\text{SF}}, \quad (5)$$

where $\text{SF} \in \{7, \dots, 12\}$ represents the Spreading Factor (SF) [15]. Therefore, the SF formally defines the number of chirps encoded per symbol, and directly determines the symbol duration and the data rate [16]. As the SF increases, the symbol duration increases and the data rate decreases. At the same

TABLE I: LoRa parameters for different SFs, with $B = 125$ kHz, $p_s = 32$ bytes, explicit header mode, and code rate equal to 2.

SF	DR	Data rate [kbit/s]	Sensitivity [dBm]	Time on air [ms]
7	5	5.470	-130.0	74
8	4	3.125	-132.5	136
9	3	1.760	-135.0	247
10	2	0.980	-137.5	493
11	1	0.440	-140.0	888
12	0	0.250	-142.5	1777

time, the receiver sensitivity improves, and so the range of the signal increases [17]. This is especially important in the NTN-IoT scenario, where EDs tend to increase the SF to maximize the communication range. Assuming $B = 125$ kHz, a PHY payload size p_s of 32 bytes, explicit header mode, and code rate equal to 2, the data rates (and Data Rate (DR) index), sensitivity, and time on air vary significantly based on the SF, as reported in Table I.

A key feature of the LoRa modulation is that SFs are pseudo-orthogonal, so that multiple signals at different data rates (i.e., using different SFs) on the same channel (i.e., using the same time/frequency resources) can be received simultaneously. In practice, successful decoding is still possible as long as the desired signal has a sufficiently higher power (generally about 6 dB higher) than the interfering signals [18].

Formally, LoRa operates at the physical layer, and is usually combined with LoRaWAN for the implementation of the rest of the protocol stack, especially the Medium Access Control (MAC) layer. While LoRa transceivers available today can operate in licensed bands between 137 MHz and 1020 MHz, they generally use the sub-GHz Industrial, Scientific, and Medical (ISM) bands (i.e., 433 MHz and 868 MHz in Europe, and 915 MHz in North America) [17].

C. Channel Model

The channel between the EDs and the LEO satellite is modeled based on the 3GPP TR 38.811 specifications [14]. The path loss (PL) consists of the free-space path loss (FSPL) and additional attenuation components, and is derived as

$$PL = 20 \log_{10} \left(\frac{4\pi d}{\lambda} \right) + L_a + CL + SF, \quad (6)$$

where d is the distance, λ is the wavelength, L_a is the atmospheric loss, SF is the shadowing, and CL is the clutter loss that accounts for building obstructions. In Line of Sight (LOS) conditions, this latter term is typically negligible, and set to 0 dB [14]. The shadowing is modeled as a zero-mean log-normal random variable with variance σ_s^2 , where σ_s depends on the environment, elevation angle, and other link-specific factors.

The atmospheric loss is due to several contributions, such as gas attenuation, rain and cloud attenuation, tropospheric scintillation, and ionospheric scintillation [14]. However, as LoRa mainly operates in sub-GHz ISM bands, only the latter component has a significant impact and is included in our model. This term is computed according to the Gigahertz

Scintillation Model [19], which is valid only for geographical regions with a maximum latitude of 20° . Hence, L_a is given by

$$L_a = \left(\frac{f_c}{4} \right)^{-1.5} \frac{P_f (4 \text{ GHz})}{\sqrt{2}}, \quad (7)$$

where f_c is the carrier frequency, and P_f (4 GHz) is a scaling factor representing the ionospheric attenuation level at 99% of the time observed in Hong Kong between March 1977 and March 1978 at a frequency of 4 GHz [14].

The received power P_{rx} (in dB) can be expressed as

$$P_{rx} = P_{tx} + G_{tx} + G_{rx} - PL, \quad (8)$$

where P_{tx} is the transmit power (in dB), and G_{tx} and G_{rx} are the transmit and receive antenna gains (in dBi), respectively.

At the beginning of the simulation, each ED is assigned a SF according to the gateway sensitivity. Specifically, we assign the lowest possible SF that guarantees that the received power P_{rx} in Eq. (8) is higher than the gateway sensitivity.

III. SIMULATION FRAMEWORK

Ns-3 is one of the most cited and advanced discrete-event network simulators. Unlike link-level simulators, which often simplify network protocols to reduce the computational complexity, ns-3 incorporates accurate models of the entire stack, enabling full-scale end-to-end simulations. In this paper, we develop a new module called ns3-LoRa-NTN to simulate NTN-IoT networks based on LoRa. This module combines the LoRa PHY/MAC stack from ns3-LoRa with the satellite channel and antenna models from ns3-NTN, adding support for end-to-end NTN-IoT simulations that were not possible with either module alone. Specifically, the ns3-NTN¹ module [20] is an open-source extension of the ns-3 simulator, developed to model NTN communication based on 3GPP Release 17 specifications. The core of the module is the implementation of the 3GPP TR 38.811 satellite channel model [14], which extends the terrestrial channel model defined in TR 38.901 [21]. The model supports multiple propagation environments (e.g., urban, suburban, rural), each associated with specific path loss, LOS probability, and fast fading profiles. It accounts for atmospheric absorption, modeled using a simplified version of the ITU-R P.676 specification [22], and scintillation effects, which are derived from tropospheric and ionospheric models [19]. In line with the 3GPP specifications, ns3-NTN includes antenna models for circular aperture antennas for satellite terminals, and Uniform Planar Array (UPA) and Very Small Aperture Terminal (VSAT) antennas for EDs [14]. Moreover, the module implements a Geocentric Cartesian coordinate (ECEF) system, to consider the Earth's curvature, as well as the elevation angle, to represent the position of a node. The x-y plane defines the equatorial plane, with the x-axis pointing at 0° longitude, the y-axis pointing at 90° longitude, and the z-axis pointing at the geographical North Pole. Finally, it extends the benchmark ns-3 code to model the propagation delay between end nodes

TABLE II: Simulation parameters.

Parameter	Value
Satellite altitude (h) [km]	[200, ..., 700]
Transmit power (P_{tx}) [dBm]	14
Bandwidth (B) [kHz]	125
Carrier frequency (f_c) [MHz]	868
ED density (ρ_d) [EDs/km ²]	0.01
Antenna beamwidth (θ) [°]	{5, 10, 15}
Total antenna gain ($G_{tx} + G_{rx}$) [dBi]	{5, 10}
Transmission periodicity (p) [s]	{60, 30, 10}
PHY payload size (p_s) [bytes]	32
Earth's radius (R_E) [km]	6371

(which is typically negligible for terrestrial links), and a Timing Advance (TA) mechanism to compensate for this delay during scheduling [23]. Radio Resource Control (RRC) and Hybrid Automatic Repeat reQuest (HARQ) timers have also been properly adjusted to account for the long propagation delay [24].

The ns3-LoRa² module is an open-source ns-3 framework to simulate LoRa networks at various levels [2]. It supports the simulation of class A EDs, in which each ED transmits application packets on the wireless channel asynchronously. After each uplink transmission, the node opens up at most two reception windows, waiting for any command or data packet returned by the Network Server (NS). The system takes into account channel interference, and considers a packet delivered successfully only if the equalized interfering power is below the channel rejection parameter defined in [25]. Additionally, it integrates both energy harvesting and consumption models, and allows for flexible network configuration, such as enabling or disabling the duty cycle restriction at the gateway. Furthermore, this module enables EDs to freely select the SF and channel for the reception windows, with no restrictions on the values specified by the LoRaWAN standard. However, ns3-LoRa does not support simulations in the NTN scenario, which motivates our research work in this paper.

The ns3-LoRa-NTN module is the first open-source module able to simulate an NTN-IoT network, where terrestrial EDs communicate with a satellite gateway, thereby expanding the scope of traditional LPWAN applications.

IV. PERFORMANCE EVALUATION

In this section, we first describe our simulation setup and parameters. Then, we present some results to validate the NTN-IoT paradigm using LoRa.

A. Simulation Setup

We run simulations using the ns3-LoRa-NTN module described in Sec. III, and simulation parameters are provided in Table II. We consider a rural scenario where N EDs are uniformly distributed on the Earth's surface with a fixed spatial density $\rho_d = 0.01$ EDs/km². A single LEO satellite, at altitude h , serves as a LoRa Gateway (GW), collecting uplink traffic from the EDs, and forwarding it to the NS for storage or processing. Each ED transmits packets of fixed

¹<https://gitlab.com/mattiasandri/ns-3-ntn/-/tree/ntn-dev>

²<https://github.com/signetlabdei/lorawan>

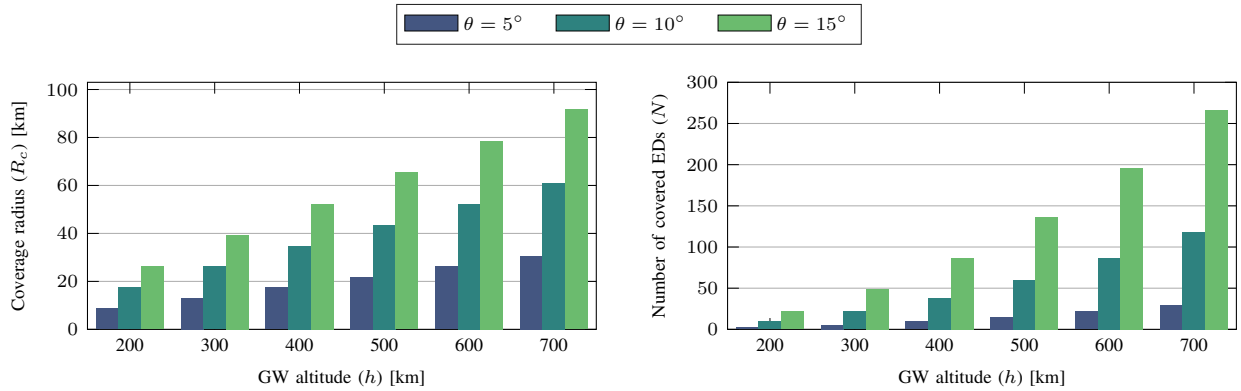
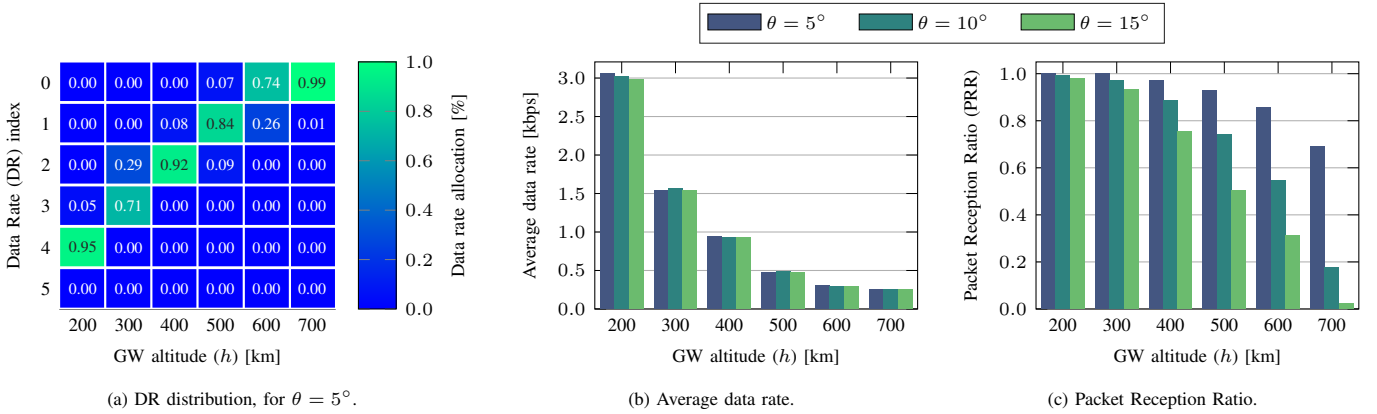


Fig. 1: Coverage radius (left) and the number of covered EDs (right) vs. θ and h , with $p = 60$ s.



(a) DR distribution, for $\theta = 5^\circ$.

(b) Average data rate.

(c) Packet Reception Ratio.

Fig. 2: DR distribution, average data rate, and PRR vs. h and θ , with $G_{tx} + G_{rx} = 5$ dBi and $p = 60$ s.

size $p_s = 32$ bytes at regular intervals with a transmission periodicity of p . The transmit power is fixed to $P_{tx} = 14$ dBm, and the bandwidth is $B = 125$ kHz [26]. As far as the antenna model is concerned, several studies, including [27], [28], assume that the antenna gain for LoRa GWs is approximately $G_{rx} = 5$ dBi, while EDs transmit via isotropic-like antennas due to energy and space constraints, so $G_{tx} = 0$ dBi. In contrast, the authors of [29] and [30] proposed an enhanced antenna model for LoRa GWs and EDs in the ISM band with a maximum gain of $G_{tx} = 8.5$ dBi and $G_{rx} = 1.9$ dBi, respectively, so we have $G_{tx} + G_{rx} \simeq 10$ dBi. Therefore, in this study we consider both models, to evaluate the impact of different antenna configurations on the network.

Simulation results are given as a function of the satellite altitude h , the antenna beamwidth θ , and the transmission periodicity p , in terms of: (i) the number of covered EDs N , the coverage radius R_c (the ground-projected radius of the satellite footprint); (iii) the DR distribution; and (iv) the PRR and average data rate.

B. Coverage Analysis

In Fig. 1 we plot the satellite's coverage radius (R_c) and the number of EDs it can serve (N), both of which depend on the satellite altitude h and the antenna beamwidth θ . Indeed, from Eq. (1), R_c increases with both h and θ . For instance, at a satellite altitude of $h = 200$ km, a beamwidth of $\theta = 5^\circ$ results in a coverage radius of approximately 10 km, while

increasing θ to 15° expands the radius to around 25 km. At higher altitudes, the coverage area grows further; for example, at $h = 700$ km and $\theta = 15^\circ$, $R_c \simeq 90$ km. Given that the device density ρ_d is fixed, from Eq. (2), the number of covered EDs N is directly proportional to the coverage area A_c . For example, with $h = 700$ km and $\theta = 5^\circ$, the satellite covers approximately 30 EDs, vs. 267 EDs for $\theta = 15^\circ$.

C. Limited Antenna Gain

In this analysis, the total antenna gain is set to $G_{tx} + G_{rx} = 5$ dBi, which reflects the typical gain used in standard LoRa gateway configurations [27], [28]. Fig. 2a illustrates the DR distribution (which directly depends on the corresponding SF, as reported in Table I), for a beamwidth of $\theta = 5^\circ$, as a function of the satellite altitude h . On one side, increasing the altitude expands the satellite's coverage area. On the other side, the resulting longer communication distance introduces more path loss, which degrades the signal quality. As such, EDs are forced to use a higher SF to operate at lower sensitivity and increase the coverage range, so the resulting DR index decreases. For instance, at $h = 200$ km, approximately 95% of the EDs operate with DR = 4 (SF = 8), and the corresponding average data rate is about 3 kbps, as shown in Fig. 2b. For $h > 500$ km, most EDs select DR = 0, and use the same SF = 12, which significantly increases the probability of collision. The corresponding average data rate is only 300 bps. At $h = 700$ km, nearly all EDs operate with DR = 0.

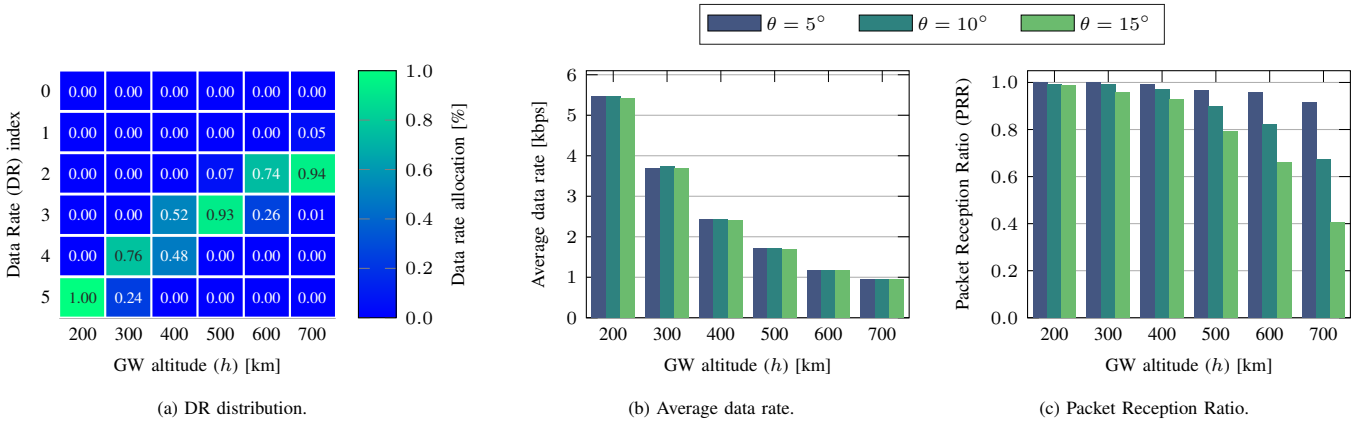


Fig. 3: DR distribution, average data rate, and PRR vs. h and θ , with $G_{tx} + G_{rx} = 10$ dBi and $p = 60$ s.

Moreover, the impact of the beamwidth θ is not negligible. As θ increases, the number of covered EDs N also increases, so the PRR decreases, as illustrated in Fig. 2c. For example, see that the PRR drops to approximately 0.7 for $\theta = 5^\circ$ (where $N = 30$), and further decreases to just 0.02 for $\theta = 15^\circ$ (where $N = 267$). This degradation occurs because the probability of packet collision increases with N , especially when many EDs use the same SF. Naturally, this behavior also depends on h . For instance, at $h = 400$ km and with $\theta = 5^\circ$, the satellite footprint has a radius of approximately 17 km, covering only about $N = 10$ EDs, so the PRR is 0.97. In contrast, with $h = 700$ km, the radius increases to approximately 30 km and $N = 30$ EDs, so the PRR decreases to 0.7.

D. Enhanced Antenna Gain

Now, we evaluate the network performance assuming a total antenna gain of $G_{tx} + G_{rx} = 10$ dBi, thereby using the enhanced configuration proposed in [29] and [30]. As shown in Fig. 3a, the additional antenna gain significantly improves the link quality compared to the scenario in Sec. IV-C. At an altitude of $h = 200$ km, all EDs select DR = 5 (SF = 7), corresponding to the highest data rate supported by LoRa (approximately 5.47 kbps), as illustrated in Fig. 3b. Even at $h = 300$ km, 24% of the EDs still maintain DR = 5, while the rest switch to a slightly lower DR index (i.e., higher SF) to satisfy the sensitivity requirements of the gateway. From $h = 400$ km, DR = 5 is no longer feasible due to more severe path loss. A notable improvement with respect to the previous scenario is observed at $h = 500$ km: in these conditions, most EDs operate with DR = 3 (SF = 9) when $G_{tx} + G_{rx} = 10$ dBi, in contrast to DR = 1 when $G_{tx} + G_{rx} = 5$ dBi. The resulting data rate increases by more than two times, from around 1 kbps to 2.5 kbps. The PRR also improves to around 0.8, vs. 0.5. At $h = 600$ km, DR = 2 (SF = 10) becomes the most common selection, so the average data rate decreases to only 1.8 kbps. Nevertheless, the PRR remains around 0.91 for $\theta = 5^\circ$, and approximately 0.66 when $\theta = 15^\circ$.

Finally, in Fig. 4 we investigate the capacity of LoRa as a function of the traffic. Specifically, we change the transmission periodicity p from 60 to 10 s so that, given a fixed payload of $p_s = 32$ bytes, the resulting source rate increases accordingly.

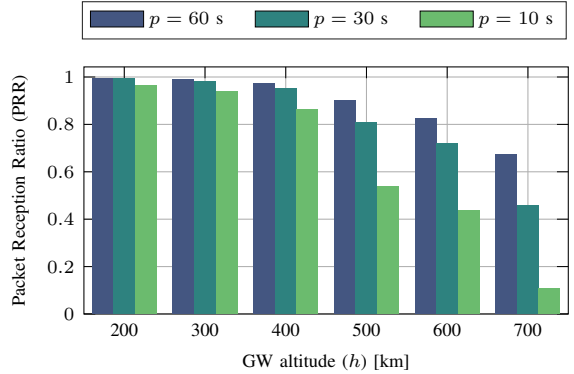


Fig. 4: PRR vs. p and h , with $G_{tx} + G_{rx} = 10$ dBi and $\theta = 10^\circ$.

This is consistent with the analysis in [31], where the authors change the source rate from 1 packet every second to 1 packet every 100 seconds. As expected, the PRR decreases as the traffic increases. However, while the degradation is as small as 2.5% at $h = 200$ km, it is up to 85% at $h = 700$ km. The impact of h is twofold. First, as h increases, the number of EDs N within the satellite footprint increases, so the network is more congested due to more frequent transmission attempts. Second, as h increases, the round-trip delay and the effective time on air of data packets increase. Given that LoRaWAN uses ALOHA for channel access, the probability of packet collisions also increases during that time, thereby reducing the PRR. For example, for $p = 60$ s, the ED source rate is 4 bps. When $h = 700$ km and $\theta = 10^\circ$, we have $N \simeq 120$ EDs, so the total source rate is around 480 bps. For $p = 10$ s, the total source rate increases to around 3 kbps. In turn, the average data rate of LoRa is 950 bps \ll 3 kbps (see Fig. 3b), that now the network cannot sustain.

These results confirm that LoRa networks can effectively operate in NTN environments, particularly when enhanced antenna configurations are employed. The additional gain extends the feasible operating altitude of the LEO satellite, and improves network robustness, even in scenarios where many EDs are covered. The performance can be further improved by leveraging the quasi-orthogonal nature of SFs. For example, EDs can spread across different SFs to reduce the impact of collisions, regardless of the value of the sensitivity, especially

in the limited antenna gain scenario, and for $h < 400$ km, when all EDs would otherwise select the same SF.

V. CONCLUSIONS AND FUTURE WORK

In this work we evaluated the feasibility of LoRa LPWANs integrated with NTN. Using an extended version of the ns3-LoRa module that incorporates the 3GPP NTN channel model, we assessed the end-to-end performance of a scenario where a single LEO satellite acts as a LoRa gateway for rural IoT deployments. Our results show that both the satellite altitude and the antenna beamwidth significantly influence coverage, data rate, and PRR. We observed that increasing the gateway altitude extends the satellite's footprint, thereby enlarging the coverage area. However, this also leads to higher path loss, which forces end devices to select higher SFs. As a result, the time on air increases, and so do the probability of packet collision and the network congestion.

As part of our future work, we will address current limitations by improving the SF selection strategy to reduce the collision probability in dense NTN scenarios. In addition, we plan to enhance our simulation framework by including multi-satellite and multi-layered NTN configurations, along with a realistic satellite mobility.

ACKNOWLEDGMENTS

This work has been partially funded by ESA within the framework of the SatNex V project, Activity INVENTIVE. The views expressed herein can in no way be taken to reflect the official opinion of ESA. The authors would like to thank Dr. Maria Rita Palattella and Prof. Giovanni Giambene for their valuable expertise and technical support throughout the preparation of this work. This work was also partially supported by the European Commission through the European Union's Horizon Europe Research and Innovation Programme under the Marie Skłodowska-Curie-SE, Grant Agreement No. 101129618, UNITE. This research was also partially supported by the European Union under the Italian National Recovery and Resilience Plan (NRRP) of NextGenerationEU, partnership on "Telecommunications of the Future" (PE0000001 - program "RESTART").

REFERENCES

- [1] B. Safaei, A. M. H. Monazzah, M. B. Bafroei, and A. Ejlali, "Reliability side-effects in internet of things application layer protocols," in *2nd International Conference on System Reliability and Safety (ICRSR)*, 2017.
- [2] D. Magrin, M. Centenaro, and L. Vangelista, "Performance evaluation of LoRa networks in a smart city scenario," in *IEEE International Conference on Communications (ICC)*, 2017.
- [3] A. P. Matz, J.-A. Fernandez-Prieto, J. Cañada-Bago, and U. Birkel, "A Systematic Analysis of Narrowband IoT Quality of Service," *Sensors*, vol. 20, no. 6, Mar. 2020.
- [4] G. G. L. Ribeiro, L. F. d. Lima, L. Oliveira, J. J. P. C. Rodrigues, C. N. M. Marins, and G. A. B. Marcondes, "An Outdoor Localization System Based on SigFox," in *IEEE 87th Vehicular Technology Conference (VTC Spring)*, 2018.
- [5] A. Chaoub *et al.*, "6G for Bridging the Digital Divide: Wireless Connectivity to Remote Areas," *IEEE Wireless Communications*, vol. 29, no. 1, pp. 160–168, Feb. 2022.
- [6] M. Giordani and M. Zorzi, "Non-Terrestrial Networks in the 6G Era: Challenges and Opportunities," *IEEE Network*, vol. 35, no. 2, pp. 244–251, Dec. 2021.
- [7] M. Vaezi *et al.*, "Cellular, Wide-Area, and Non-Terrestrial IoT: A Survey on 5G Advances and the Road Toward 6G," *IEEE Communications Surveys & Tutorials*, vol. 24, no. 2, pp. 1117–1174, 2022.
- [8] H. Mroue, A. Nasser, S. Hamrioui, B. Parrein, E. Motta-Cruz, and G. Rouyer, "MAC layer-based evaluation of IoT technologies: LoRa, SigFox and NB-IoT," in *IEEE Middle East and North Africa Communications Conference (MENACOMM)*, 2018.
- [9] G. Sciddurro *et al.*, "Looking at NB-IoT Over LEO Satellite Systems: Design and Evaluation of a Service-Oriented Solution," *IEEE Internet of Things Journal*, vol. 9, no. 16, pp. 14 952–14 964, Aug. 2022.
- [10] M. Afhamis and M. R. Palattella, "SALSA: A Scheduling Algorithm for LoRa to LEO Satellites," *IEEE Access*, vol. 10, pp. 11 608–11 615, Jan. 2022.
- [11] G. Boquet, P. Tuset-Peiró, F. Adelantado, T. Watteyne, and X. Vilajosana, "LR-FHSS: Overview and Performance Analysis," *IEEE Communications Magazine*, vol. 59, no. 3, pp. 30–36, Mar. 2021.
- [12] A. Guidotti, A. Vanelli-Coralli, A. Mengali, and S. Cioni, "Non-terrestrial networks: Link budget analysis," in *IEEE International Conference on Communications (ICC)*, 2020.
- [13] D. Wang, A. Traspadini, M. Giordani, M.-S. Alouini, and M. Zorzi, "On the Performance of Non-Terrestrial Networks to Support the Internet of Things," in *56th Asilomar Conference on Signals, Systems, and Computers*, 2022, pp. 881–887.
- [14] 3GPP, "Study on New Radio (NR) to Support Non-terrestrial Networks (Release 16)," 3rd Generation Partnership Project (3GPP), Technical Report TR 38.811, 2020.
- [15] N. Hou, X. Xia, and Y. Zheng, "Don't Miss Weak Packets: Boosting LoRa Reception with Antenna Diversities," *ACM Trans. Sen. Netw.*, vol. 19, no. 2, Feb. 2023.
- [16] Z. Sun, H. Yang, K. Liu, Z. Yin, Z. Li, and W. Xu, "Recent Advances in LoRa: A Comprehensive Survey," *ACM Trans. Sen. Netw.*, vol. 18, no. 4, Nov. 2022.
- [17] T. Voigt, M. Bor, U. Roedig, and J. Alonso, "Mitigating Inter-network Interference in LoRa Networks," in *International Conference on Embedded Wireless Systems and Networks*, 2017.
- [18] D. Croce, M. Guicciardo, S. Mangione, G. Santaromita, and I. Tinnirello, "Impact of LoRa Imperfect Orthogonality: Analysis of Link-Level Performance," *IEEE Communications Letters*, vol. 22, no. 4, pp. 796–799, Apr. 2018.
- [19] ITU, "Ionospheric Propagation Data and Prediction Methods Required for the Design of Satellite Services and Systems," *Recommendation P.531*, 2012.
- [20] M. Sandri, M. Pagan, M. Giordani, and M. Zorzi, "Implementation of a channel model for non-terrestrial networks in ns-3," in *Workshop on ns-3*, 2023.
- [21] 3GPP, "Study on Channel Model for Frequencies from 0.5 to 100 GHz," 3GPP, TR 38.901, 2020.
- [22] ITU, "Attenuation by atmospheric gases and related effects," *Recommendation P.676*, 2013.
- [23] 3GPP, "NR – Physical Layer Procedures for Data (Release 15)," 3GPP, TS 38.214, 2018.
- [24] ———, "Solutions for NR to support Non-Terrestrial Networks (NTN) (Release 16)," TR 38.821, 2020.
- [25] C. Goursaud and J. M. Gorce, "Dedicated networks for IoT: PHY / MAC state of the art and challenges," *EAI Endorsed Transactions on Internet of Things*, vol. 1, no. 1, Nov. 2015.
- [26] J. Petajajarvi, K. Mikhaylov, A. Roivainen, T. Hanninen, and M. Petäjäsalo, "On the coverage of LPWANs: Range evaluation and channel attenuation model for LoRa technology," in *14th International Conference on ITS Telecommunications (ITST)*, 2015, pp. 55–59.
- [27] A. Rahman and M. Suryanegara, "The development of IoT LoRa: A performance evaluation on LoS and Non-LoS environment at 915 MHz ISM frequency," in *International Conference on Signals and Systems (ICSigSys)*, 2017.
- [28] Adnan, A. E. U. Salam, A. Arifin, and M. Rizal, "Forest Fire Detection using LoRa Wireless Mesh Topology," in *East Indonesia Conference on Computer and Information Technology (EIConCIT)*, 2018.
- [29] E. Palantei *et al.*, "A 923 MHz Steerable Antenna for Low Power Wide Area Network (LPWAN)," *IEEE International Conference on Communication, Networks and Satellite (Comnetsat)*, 2020.
- [30] M. S. Yahya *et al.*, "Triple-Band Reconfigurable Monopole Antenna for Long-Range IoT Applications," *Sensors*, vol. 23, no. 12, Jun. 2023.
- [31] D. Magrin, M. Capuzzo, and A. Zanella, "A Thorough Study of LoRaWAN Performance Under Different Parameter Settings," *IEEE Internet of Things Journal*, vol. 7, no. 1, pp. 116–127, Jan. 2020.